Organic Electronics 98 (2021) 106290

Contents lists available at ScienceDirect

Organic Electronics

journal homepage: www.elsevier.com/locate/orgel

A wearable and highly sensitive capacitive pressure sensor integrated a dual-layer dielectric layer of PDMS microcylinder array and PVDF electrospun fiber

Ming-Feng Lin [a], Chia Cheng [a], Ching-Ching Yang [b], Wen-Tse Hsiao [b,**], Chii-Rong Yang [a,*]

[a] Department of Mechatronic Engineering, National Taiwan Normal University, 162, Sec. 1, Ho-Ping E. Road, Taipei, 106, Taiwan, ROC
[b] Taiwan Instrument Research Institute, National Applied Research Laboratories, 20 R&D Road VI, Hsinchu Science Park, Hsinchu city 300, Taiwan, ROC

ARTICLE INFO

Keywords:
Flexible capacitive pressure sensor
sensitivity
Electrospinning
Microcylinder structure
Dual-layer dielectric

ABSTRACT

Recently, high-performance flexible pressure sensors have received considerable attention because of their potential application in fitness tracking, human–machine interfaces, and artificial intelligence. Sensitivity is a key parameter that directly affects a sensor's performance; therefore, improving the sensitivity of sensors is a vital research topic. This study developed a dual-layer dielectric structure comprising a layer of electrospun fiber and an array of microcylinders and used it to fabricate a novel high-sensitivity capacitive pressure sensor. A simple, rapid, low-cost, and controllable microstructured method that did not require complex and expensive equipment was adopted. The proposed sensor can efficiently detect capacitance changes by analyzing changes in the fiber and microcylinder structure when compressed. It has high sensitivity of 0.6 kPa^{-1}, rapid response time of 25 ms, ultralow limit of detection of 0.065 Pa, and high durability and high reliability without any signal attenuation up to 10,000 load/unload cycles and up to 5000 bending/unbending cycles. Moreover, it yielded favorable results in real-time tests, such as pulse monitoring, acoustic tests, breathe monitoring, and body motion monitoring. Furthermore, experiments were conducted using a robotic arm, and the obtained results verify that the sensor has different capacitance responses to objects with different shapes, which is crucial for its future applications in smart machinery. Finally, the sensors were arranged as a 6 × 6 matrix, and they successfully displayed the pressure distribution in a plane. Thus, the contributions of the capacitance pressure sensor with a dual-layer dielectric structure in the field of high-performance pressure sensors were verified.

1. Introduction

Recently, due to their practical applications in human–machine interfaces, intelligent robots, touch panels, electronic skins, and health monitors, flexible pressure sensors have attracted increasing attention [1–6]. The four classic sensing mechanisms of pressure sensors are the piezoresistive effect [7–9], piezoelectricity [10–12], capacitance [1–6], and triboelectric effect [13–17]. Pressure sensors with capacitance mechanisms have structural simplicity, low power consumption, rapid response, and high reliability and stability, and they rapidly and steadily can convert external stimulations into capacitance signals. Therefore, these pressure sensors enable nonliving objects, such as robotic arms, to perceive the same sensations as human skin does during interactions. These sensors can also be integrated into wearable devices to measure human joint movements, breathing, pulse, and languages [18–22].

Classic flexible capacitive pressure sensors are a type of device formed by sandwiching an elastic dielectric layer between flexible electrodes. When pressure is applied on the sensor, the distance between the electrodes changes, which consequently affects the capacitance value. Therefore, manufacturing a three-dimensional structure on the electrode or dielectric layer is presently the main method employed to increase the compressibility and sensitivity of sensors. Studies have verified that the introduction of micropyramid [19,23–25], microwrinkle [26], microconvex [27], tilted micropillar [28], or microcylinder [29,30] structures can effectively improve sensor sensitivity. However, most of these studies have utilized single-sided structures to manufacture sensors; limitations in the morphology of these structures may afford some unimprovable shortcomings, such as limited

* Corresponding author.
** Corresponding author.
E-mail addresses: wentse@narlabs.org.tw (W.-T. Hsiao), ycr@ntnu.edu.tw (C.-R. Yang).

https://doi.org/10.1016/j.orgel.2021.106290
Received 9 February 2021; Received in revised form 18 June 2021; Accepted 11 July 2021
Available online 16 July 2021

compressibility, low durability, and increased viscoelastic behaviors. To overcome these shortcomings, double-sided structures were used as dielectric layer. Baek et al. fabricated wrinkles on both sides of polydimethylsiloxane (PDMS) dielectric layers via mechanical stretching [31]. Yoon et al. used sandpaper as a mold to fabricate irregular structures on both sides of the dielectric layer via PDMS remolding [32]. Guo et al. used anodic aluminum oxide (AAO) plates as molds to form double-sided nanocolumn dielectric layers after remolding [29]. These studies have verified that dielectric layers with double-sided structures are more sensitive than those with single-sided structures. Presently, most studies on this topic have only investigated a single material and structure or two types of heterogeneous materials to form a single structure. For example, Ma et al. used $BaTiO_3$ as an additive to improve the dielectric properties of PDMS and enhanced the sensitivity of the sensor using a micro-wrinkle structure [33]. In other words, no research exists on the integration of two types of heterogeneous materials to form a dual-layer dielectric structure to explore the possibility of capacitive sensors with high flexibility and adjustable sensitivity.

This study developed a dual-layer dielectric structure comprising a polyvinylidene difluoride (PVDF) fiber layer and PDMS microcylinder array. Moreover, its feasibility for application to capacitive pressure sensors was investigated. The high dielectric coefficient of PVDF and the air gap created by electrospinning facilitate the formation of a special bulked layer, and with the incorporation of arrayed microcylinders, a new type of dual-layer dielectric structure is obtained. Compared to dielectric layers with single-layer microcylinder structures, the synergic effects of the two heterogeneous structures can effectively overcome the previously mentioned shortcomings. When pressure is applied on the sensor, the fiber layer releases air in the gaps; even a slight pressure can change the distance between the electrodes, thus increasing the sensor's sensitivity. When the sensor is subject to high pressure, the cylinder deeply embeds into the fiber layer and continues to release the air in the fiber layer. Furthermore, it increases the density of the fiber and cylinder composite layer. This significantly changes the distance between the electrodes, resulting in capacitance changes. When the pressure on the sensor is released, the cylinders pressed into the fibers rapidly widen the distance between the electrodes. The fiber layer compressed because of the pressure rapidly returns to its original bulky state. This type of complementary outcome can increase the sensitivity of the sensor toward changes in the distance between the electrodes and afford low hysteresis, thus increasing the capacitance changes and durability of the sensors. The overall manufacturing process comprises simple and rapid PVDF electrospinning and PDMS pattern transfer methods with large surfaces and controllable microstructures without the need for complicated and expensive equipment. The prepared sensors have a multisectional tunable sensitivity of 0.6 kPa^{-1} (0–7 kPa), 0.51 kPa^{-1} (7–15 kPa), and 0.03 kPa^{-1} (15–50 kPa). Additionally, they afford rapid response time of 25 ms, ultralow limit of detection (LOD) of 0.064 Pa, and high durability and high reliability without any signal attenuation up to 10,000 load/unload cycles and up to 5000 bending/unbending cycles. Furthermore, the sensor yielded favorable results in some practical applications; for example, real-time testing of pulse monitoring, acoustic vibration detection, breathe monitoring, and body motion monitoring. The sensor attached to the gripper of the robotic arm was also evaluated for grasping actions, and the results verify that the sensor has distinguishable capacitance responses to objects with different shapes. Finally, a sensor array of 6 × 6 pixels was fabricated, which successfully projected the pressure distribution onto a flat surface. This study demonstrates the performance improvements of the capacitive sensors using dual-layer microstructured dielectric layers with heterogeneous materials, which will contribute to the development in the field of high-performance pressure sensors.

2. Experimental section

2.1. Materials

The 0.175-mm-thick polyimide (PI) film was purchased from Lih-Kuang Industry Co., Ltd. (Taiwan). Multilayer reduced graphene oxide (rGO) was purchased from LinGo-GO Co., Ltd. (Taiwan). Polydimethyldiallylammonium chloride (PDDA) was purchased from DKS Co., Ltd. (Japan). The PDMS gel (Sylgard 184) was purchased from Dow Corning (USA). The PVDF powder was purchased from Sigma-Aldrich (Germany). Photoresist (P-BZ4000) was purchased from TOK Inc. (Japan). Dimethylformamide (DMF) was purchased from Ancore Inc. (Australia).

2.2. Preparation of conductive PI/graphene films

PI film has high insulation and flexibility; thus, it is highly suitable as a substrate for flexible sensors. This study utilizes this material and coats it with graphene slurry to form a conductive film, which can be used as the electrode substrate of the sensor. To form the graphene slurry, 2 wt% rGO was added to 2 wt% PDDA solution, used as the graphene dispersant. The slurry was mixed for 24 h under room temperature to avoid graphene agglomeration. Next, a PI film was cut into 1.5 cm × 1.5 cm pieces and submerged in a 1:1 mixture of acetone and isopropanol for 30 s, and then, it was rinsed with deionized (DI) water for 1 min and blow dried with clean dry air (CDA) to ensure the complete removal of surface oils. Thereafter, the prepared graphene slurry was deposited onto the PI film via a drop-casting technique. The film was then placed on a hotplate and heated at 100 °C for 5 min to completely evaporate the moisture. The graphene layer was approximately 50 μm thick, and the sheet resistance was approximately 7.5 Ω/cm^2. The conductive PI/graphene film can provide sufficient flexibility and conductivity as the electrode base for the upper and lower parts of the capacitance sensor.

2.3. Fabrication and assembly of sensors with dual-layer dielectric structures

Sensor electrodes with PDMS microcylinder arrays and PVDF electrospun fibers were prepared using a simple and low-cost manufacturing process (Fig. 1). Fig. 1 (a) presents the manufacturing process of the electrodes with a PDMS microcylinder array structure. First, 4-inch wafers were cleaned according to standard RCA steps and were coated with a 55-μm-thick P-BZ4000 photoresist layer at 850 rpm for 30 s. Then, the wafers were prebaked at 65 °C for 3 min and soft baked at 145 °C for 5 min. They were then naturally cooled to room temperature. The wafers were exposed to 250 mJ/cm^2 of I-line UV light to define a circular pattern with a diameter of 15–45 μm and a fixed spacing of 100 μm. The wafers then underwent post exposure baking at 95 °C for 5 min and were developed with a 2.38 wt% tetramethylammonium hydroxide solution for 2 min to complete the photoresist structure with a microhole array.

Using this photoresist structure as a template for replicating the PDMS structure, an arrayed PDMS microcylinder structure was obtained. The PDMS silicone elastomer and curing agent were mixed at a 10:1 weight ratio and then mixed using a vacuum degassing mixer (MV-300S, Chaon-Guan Co., Ltd., Taiwan) for 3 min to ensure complete removal of air bubbles and uniform mixing. The mixture, or prepolymer, was spin-coated onto the previously prepared photoresist structure at 800 rpm for 30 s and then prebaked at 100 °C for 1 min. Before the solidification of PDMS, the prepared conductive PI/graphene film, on the side of the conductive graphene layer, was pressed onto PDMS with a pressure of 1 kPa and heated at 65 °C until the PDMS fully solidified. Then, the PDMS was carefully peeled off the photoresist to obtain the electrode structure with a PI/graphene/PDMS microcylinder array.

Fig. 1 (b) presents the manufacturing process of the PVDF fiber electrode. 1.8 g of PVDF powder was mixed with 6 mL of DMF, and the

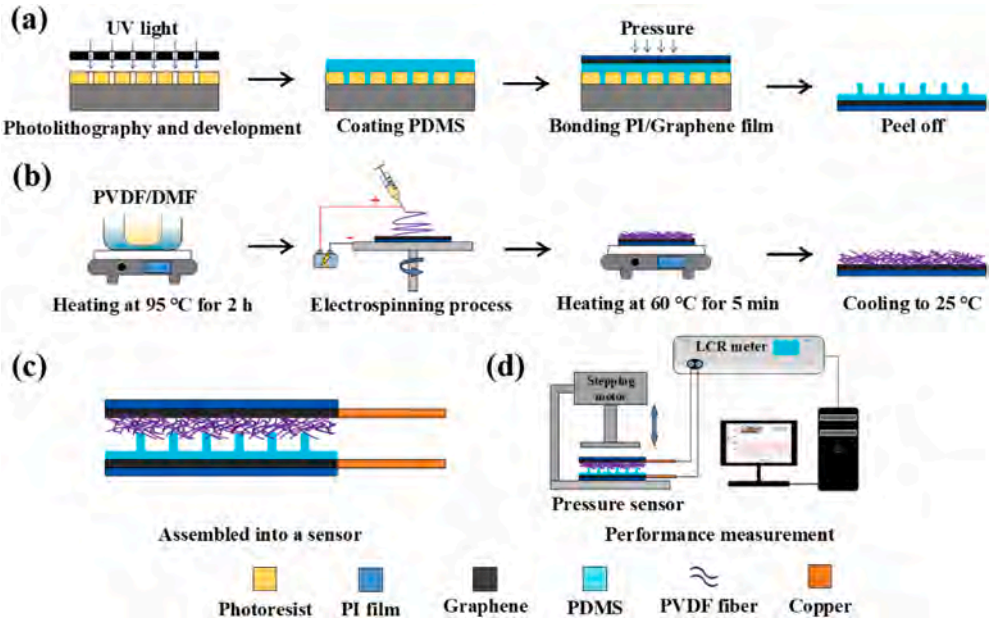

Fig. 1. Schematics of (a and b) the fabrication process of microstructured electrodes, (c) the assembled array as a capacitive pressure sensor, and (d) the performance measurement setup of the sensor.

mixture was heated in water to 95 °C with continuous stirring for 4 h to ensure that the PVDF was completely dissolved. The solution was cooled to room temperature, diluted with 4 mL of acetone, and stirred for 30 min until it was uniformly mixed. The mixed solution was left to stand for 1 h, and after confirming that no bubbles were present inside, the solution was poured into an injection syringe, which was placed inside an automatic syringe pump (KDS101, KD Scientific Inc., USA). The feed rate was set at 0.1 mL/h, and the distance between the needle tip and collecting plate was adjusted to 10 cm. With the high-voltage power supply of 10 kV and the current limited to 300 μA, the positive electrode was connected to the syringe head and the negative electrode was connected to the collecting plate. The collecting plate was rotated at 10 rpm to avoid the agglomeration of electrospun fibers from excessive concentration in the same place. The prepared conductive PI/graphene film was placed on the collecting plate (graphene side toward the needle), and the electrospinning time was 1–5 min; after completion, the conductive PI/graphene film was heated at 60 °C for 5 min until the DMF and acetone were fully volatilized. These steps were repeated five times, until 15–85-μm-thick PVDF fibers were obtained.

After preparing these two types of electrode structures, the PDMS microcylinder array and PVDF fiber electrodes were assembled by connecting the microcylinder with the fiber layer (Fig. 1 (c)). Copper tape was connected to the graphene layer to facilitate the receiving of the capacitance signal by the external measuring instruments. PI tape was attached to the edges of the sensor to ensure complete sealing. Finally, the prepared capacitance sensor was placed on the testing platform to perform various loading–unloading cycle tests (Fig. 1 (d)), wherein the impact from a Z-axis slider driven through a stepper motor was applied to the sensor, and an LCR meter was used to capture the capacitance changes in the pressure sensor during the loading–unloading cycles. The signals and data were displayed and stored on a computer for subsequent analysis.

2.4. Preparation and assembly of the sensor array

The composite dielectric layer formed using the optimal PDMS microcylinder (25 μm diameter and 55 μm height) and PVDF fiber (50 μm thickness) was used to prepare a sensor array of 6 × 6 pixels. First, two pieces of PI film were cut into 7 cm × 7 cm squares; the film pieces were submerged in a 1:1 solution of acetone and isopropanol by volume for 30 s and washed with DI water for 1 min and blow dried with CDA to ensure the complete removal of surface oils. Thereafter, six pieces of copper tape (12 cm in length and 0.5 cm in width) were attached, 0.5 cm apart, to the two cropped pieces of PI films to complete the preparation of the upper and lower electrode substrates. Furthermore, the PDMS elastomer mixed with hardener was coated onto the prepared 4-inch photoresist template at 800 rpm, which was placed on the PVDF electrospun collecting plate. Using the same electrospinning steps as before, approximately 50 μm of fiber was collected after 3 min of spinning, thus obtaining the composite PVDF fiber and microcylinder structure dielectric layer. This dielectric layer was sandwiched between the upper and lower electrodes; the copper tape on the two electrodes must touch the dielectric layer in a straight vertical line. PI tape was attached to the edges of the component to ensure that the three-layer structure (upper electrode−dielectric layer−lower electrode) was fully fixed and sealed. Thus, the 6 × 6 arrayed capacitance sensor was assembled.

2.5. Characterization and measurements

The surface morphology and sectional view of the dielectric layer were evaluated using a field emission scanning electron microscope (ZEISS Sigma 300, ZEISS) at an accelerating voltage of 5 kV. The microcylinder array structure was observed using a confocal microscope (LEXT OLS4000, OLYMPUS), and the surface resistance of the conductive graphene film was measured using a four-point probe (Keithley 2400, Tektronix Inc.). Sensor stress tests were conducted using a tensile testing machine (QC506M2F, Cometech Co., Ltd., Taiwan) connected to a computer server, and the sensor capacitance signals were captured at 300 kHz using an LCR meter (LCR-6300, GW Instek, Taiwan). A machine with a crank-slider mechanism was designed and assembled to evaluate the durability and reliability of the developed sensors. The sensor was placed on an experiment platform, and an electric motor propelled the crank-slider mechanism to strike the sensor. The sensor stability was tested at a fixed distance of 5 cm over a long period.

3. Results and discussion

3.1. Working mechanisms of sensors with the structured dielectric layer

Fig. 2 presents the schematics of the sensors with different types of

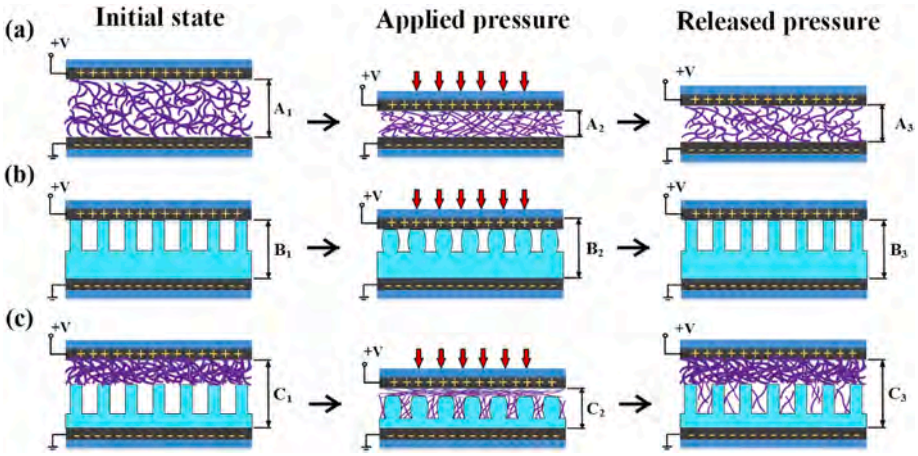

Fig. 2. Sensing mechanisms and graphical explanation of the capacitive pressure sensors with (a) pure fiber dielectric layer, (b) pure microcylinder dielectric layer, and (c) composite microcylinder and fiber dielectric layer during pressure loading and unloading.

dielectric layers during pressure loading and unloading. The pure fiber dielectric layer in Fig. 2 (a) denotes that when under load, due to a large number of holes in the fiber structure itself, even small amounts of pressure can squeeze out air and cause capacitance changes. However, after the load is released, because of insufficient tension, the fiber is unable to quickly return to its original state. This severely affects the speed and durability of the sensor's capacitance response. Conversely, Fig. 2 (b) demonstrates that when pressure is applied to a sensor with only a microcylinder dielectric layer, due to the high strength of the structure, the distance between electrodes does not easily change. Furthermore, the layer easily returns to its precompression state after the pressure is released. In this study, to address these structural shortcomings, these two types of structures were combined into a composite dielectric layer and used for sensor fabrication (Fig. 2 (c)). With both a fiber structure with many holes and a microcylinder structure, the composite dielectric layer is suitable for use under subtle pressures or high-pressure loads. When the sensor is subject to small amounts of pressure, the air in the fiber layer is released, changing the distance between the electrodes. When the load is increased, the microcylinder structure begins to embed into the fiber layer and becomes compressed, reducing the distance between the fibers and microcylinders. In addition to the changes in distance, the material density greatly increases; the dielectric coefficient of the dielectric layer changes because of the large amount of air being released. When the load is released, the strength of the microcylinders increases the distance between the electrodes, and the fiber layer with a slow restoration speed rapidly returns to its original state with support from the microcylinders (Fig. 2 (a) and (b)). This observation indicates that the integration of both structures can generate complementary effects and thereby improve the sensor performance.

Capacitance C can be calculated using the definition in equation (1) for general parallel-plate capacitance. In this equation, A is the area of overlapping electrodes in two-plate capacitors, and $\triangle d$ denotes the change in distance between the two electrodes. ε is the dielectric constant and is defined by equation (2), wherein ε_0 is the vacuum dielectric constant and ε_r is the relative dielectric constant. In this study, the overlapping area of the two electrodes A was almost fixed, and therefore, it can be considered a constant. Thus, the capacitance value is

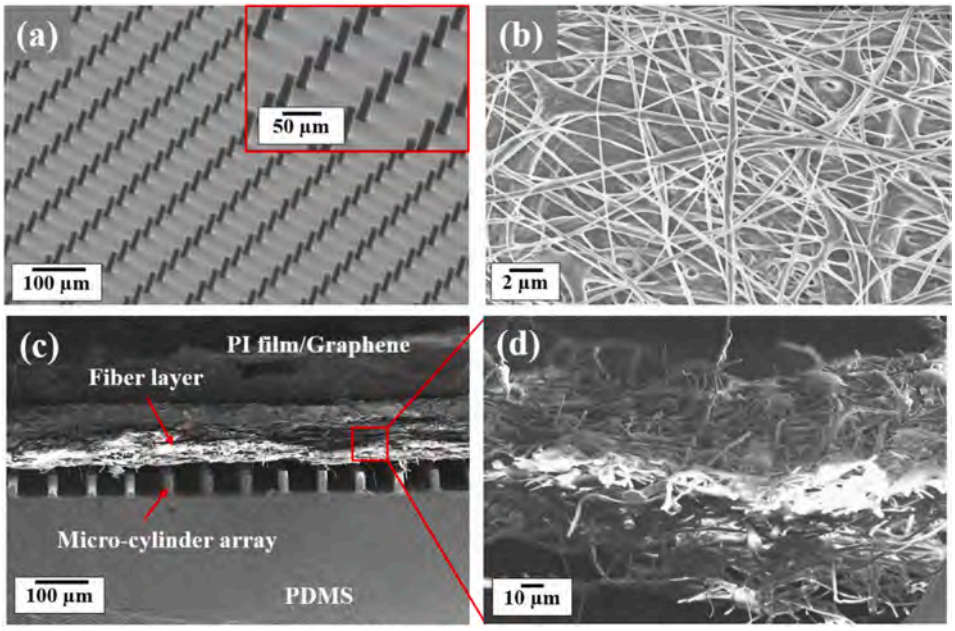

Fig. 3. SEM images of the composite dielectric layer. (a) 45° tilt-view of the microcylinder array. (b) Top-view of the electrospun fiber layer. (c) Cross-sectional view of the assembled capacitive pressure sensor. (d) Magnified view of the fiber layer in (c).

mainly affected by changes in the dielectric coefficient and the distance between the electrodes. When pressure is applied to the sensor, since microcylinders are embedded in the fiber and the fiber is compressed and thinned, the change in the distance between the two electrodes $\triangle d$ is given by $C_3 - C_2$. The densities of the fiber and microcylinder layers also increase because of the released air (Fig. 3 (c)). The relative dielectric coefficient of the dielectric layer ε_r is defined using equation (3) [29]. Here, ε_{air}, ε_{PVDF}, and ε_{PDMS} represent the relative coefficients of air, PVDF, and PDMS, respectively; V_{air}, V_{PVDF}, and V_{PDMS} represent their volumes, respectively. $\varepsilon_{air} = 1$, and ε_{PVDF} and ε_{PDMS} were approximately 10 and 3, respectively. Since the air in the dielectric layer is effectively reduced during compression, the capacitance change increases.

$$C \propto \varepsilon A / \triangle d \tag{1}$$

$$\varepsilon = \varepsilon_0 \cdot \varepsilon_r \tag{2}$$

$$\varepsilon_r = \varepsilon_{air} \cdot V_{air} + \varepsilon_{PVDF} \cdot V_{PVDF} + \varepsilon_{PDMS} \cdot V_{PDMS} \tag{3}$$

3.2. Structural feature of the dual-layer dielectric structure

Fig. 3 (a) presents the scanning electron microscopy (SEM) images of the prepared PDMS microcylinder structure electrode, and the inset is the microcylinder magnified 400 times. Since PDMS can be easily remolded, arrayed microcylinder structures with a large area and adjustable dimension can be quickly manufactured using a patterned photoresist as a template. The SEM image shows that these microcylinders have highly reproducible morphology, indicating that the overall remolding process was successful. Fig. S1 presents a laser confocal microscopy image of the microcylinders, this indicates the average height and diameter of the microcylinders were controlled at 55 and 24.5 μm, respectively. Fig. 3 (b) shows the top view of the PVDF fiber electrode. Since a rotating collector plate was used during electrospinning, the fibers were evenly distributed, with no excessive clustering at one place. The SEM images indicate that the average fiber diameter was approximately 0.8 μm. Fig. 3 (c) presents a sectional view of the capacitance pressure sensor after packaging. Fig. 3 (d) shows the enlarged image of the fiber layer in Fig. 3 (c). The many gaps present between the fibers store air, and when pressure is applied to the sensor, the microcylinders are embedded into the fiber layer and air is rapidly expelled. As pressure is released, the cylinders in the bottom electrode enable the compressed fiber layer to rapidly return to its original fluffy state, such mechanisms impart a sponge-like elasticity to the sensor.

3.3. Evaluation of sensor performance and characteristic

Sensitivity is a key parameter that directly affects a sensor's performance. Pressure sensitivity, S, is defined using equation (4), where C_0 is the initial capacitance value before the load is applied, and $\triangle C$ is the relative capacitance difference, $C - C_0$ (where C is the capacitance after pressure is applied). P is the applied external pressure. From the tangent slope of the pressure–capacitance curve, the sensitivity S of the sensor can be calculated.

$$\boldsymbol{S} = \frac{\boldsymbol{\delta}(\boldsymbol{\Delta C}/\boldsymbol{C_0})}{\boldsymbol{\delta P}} \tag{4}$$

Since the fabrication process used herein enables a high degree of size control, we assessed the changes in pressure sensitivity using microcylinders with different diameters and electrospun fibers with different thicknesses. The density and height of microcylinders influence the sensitivity of the proposed sensor. A previous study indicated that sparse microstructures can suffer from a bigger loading pressure than dense microstructures [30], which will make the deformation of the structure easier. A taller cylinder can afford better bendability to the structure, which is beneficial for increasing sensitivity. In this study, from the perspective of fixing cylinder spacing and highness, the diameter of the cylinders was used to control the density and aspect ratio of the cylinder arrays to improve the sensitivity of the proposed sensors. The height of the microcylinders was fixed to 55 μm, which was the thickness limit of the P-BZ4000 photoresist in a single-layer coating. When the diameters of the microcylinders were changed from 15 to 40 μm, the density and aspect ratio of the microcylinders varied. Since the spacing between the microcylinders was fixed to 100 μm, the density increased with the diameter. Furthermore, the density of the microcylinders affects the squeezed degree of the dielectric layer. For example, Fig. S2 compares the sensitivity of flexible capacitive pressure sensors with different diameters of PDMS microcylinder dielectric layers. The results reveal that the microcylinder dielectric layer with a diameter of 25 μm had a relatively high sensitivity of 0.39 kPa^{-1}. The cylinders with diameters of 15 and 40 μm little influenced the change in the distance between the electrodes as pressure was applied, yielding low pressure sensitivities of 0.06 and 0.07 kPa^{-1}, respectively. When the diameter of the cylinder is 40 μm, the cylinders are arranged closer to each other and have higher density. Thus, each cylinder suffers from smaller loading pressure, which is not conducive to compression or bending deformation. Consequently, the sensitivity of the sensor decreases. In contrast, when the diameter of the cylinder is 15 μm, the high aspect ratio and low density make the cylinders extremely fragile and easy to deform. However, this weak structure cannot support the weight of the electrode, and it instead reduces the sensitivity.

Furthermore, for the electrospinning times, the same PDMS microcylinders with a diameter of 25 μm and a spacing of 100 μm were used as structured electrodes. A sensor integrated with the PDMS microcylinder array and 3 min electrospun PVDF fiber has the highest pressure sensitivity of 0.6 kPa^{-1} (Fig. S3); this sensitivity is substantially greater than the sensitivities observed after 1 and 5 min of electrospinning (0.18 and 0.06 kPa^{-1}, respectively). These findings can be explained as follows. An extremely short electrospinning time results in insufficient fiber thickness, which does not considerably increase the pressure sensitivity; however, when the electrospinning time is too long, the PVDF fiber, before drying, condenses into liquid beads due to the surface tension, resulting in clumping and an uneven fiber layer. This significantly influences the pressure sensitivity and must be completely avoided.

After the experiment parameters were optimized, the pressure–capacitance curves for sensors with different microstructured dielectric layers (such as flat, fiber, microcylinder, and fiber/microcylinder composite dielectric layer) were compared (Fig. 4 (a)). The sensor with a fiber/microcylinder composite dielectric layer demonstrated an ultrahigh sensitivity of 0.6 kPa^{-1} at a low pressure range of 0–7 kPa. This is 4 or 1.5 times higher than the values of sensors with only fiber or microcylinder structured dielectric layer (0.15 and 0.39 kPa^{-1}), respectively, and as much as 20 times higher than the sensor with a flat dielectric layer (0.03 kPa^{-1}). This is because PVDF has a higher dielectric coefficient and the fluffiness of the fiber structure layer combined with the support from the microcylinder increases the sensitivity of the sensor. Fig. S4 also shows that at a medium pressure range of 7–15 kPa, a high sensitivity of 0.51 kPa^{-1} was achieved for the proposed sensor; at a high pressure range of 15–50 kPa, the sensitivity was 0.03 kPa^{-1}. The results reveal that the proposed sensor exhibits different levels of sensitivity at different pressure ranges, indicating that the sensor has outstanding tunability and is suitable for diverse applications that require different sensitivity levels.

Fig. 4 (b) presents the lowest LOD of the sensor, which has with a fiber/microcylinder composite dielectric layer. When the pressure was less than 0.0065 Pa, almost no change was observed in the capacitance. However, when the load was increased to 0.065 Pa (approximately 15 mg), the sensor exhibited small capacitance changes. This finding indicates that the lowest pressure that can be detected by the sensor is 0.065 Pa. The proposed sensors are influenced by noise (about 0.0–0.15 pF). This can be identified when the sensor is not stimulated by an external pressure. Its baseline capacitance change with noise is about 0.0–0.15 pF, as shown from the first 15 s of Fig. 4. (b). Hence, when the

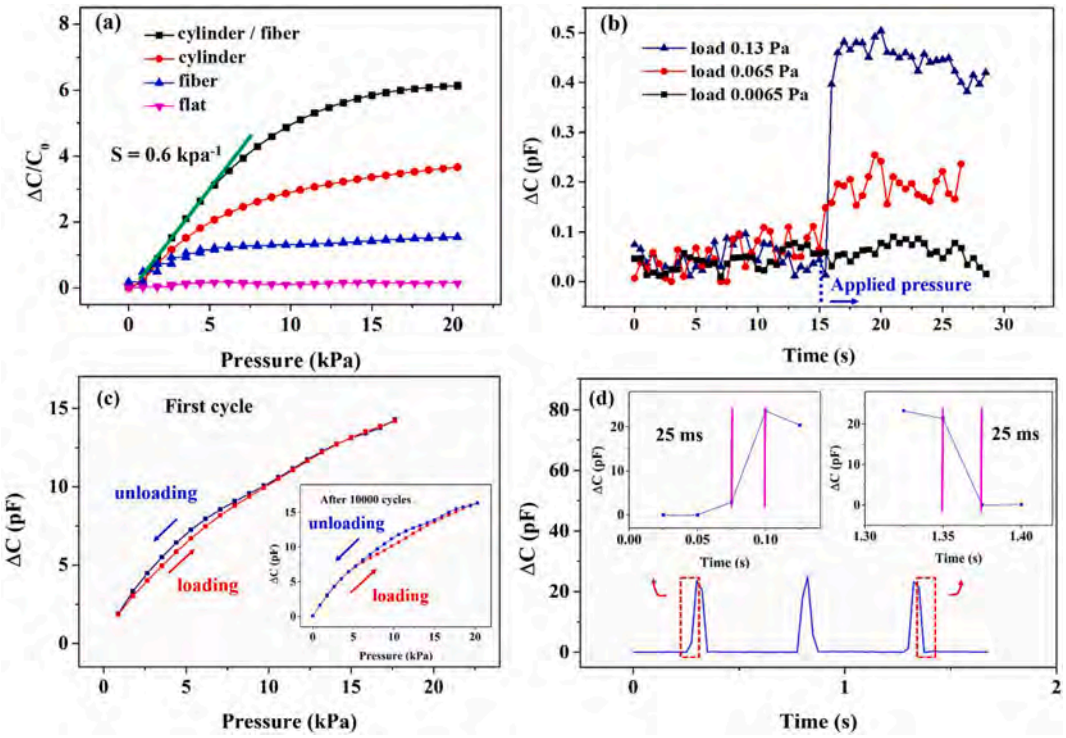

Fig. 4. (a) Sensitivity comparison of capacitive pressure sensors with different type of dielectric layers. (b) LOD with an ultralow pressure of ~0.065 Pa. (c) Hysteresis characteristics of the pressure sensor under the first cycle and after 10000 cycles. (d) Response time of the pressure sensor.

capacitance change signal is larger than 0.15 pF (signal-to-noise ratio > 1), the LOD can be distinguished, as 0.065 Pa in Fig. 4. (b). This ultralow pressure detection is facilitated by the fiber layer's air gaps, which can exhaust air under an ultralow pressure, causing slight changes in the electrode spacing that affects the capacitance value. When the load was increased to 0.13 Pa, the capacitance changes became more evident.

Fig. 4 (c) presents the hysteresis curves of the first and 10,000th pressure load–unload cycles during the sensor testing. The results indicate that during the first cycle, the capacitance response curves for loading and unloading were only slightly different, and therefore, the hysteresis effect could be ignored. After the 10,000th load–unload pressure cycle, although a slight hysteresis region was still produced, the capacitance response curve exhibited high reproducibility. This verified that the dual-layer dielectric structure of a fluffy PVDF fiber film and an arrayed PDMS microcylinder produces synergic effects, which can effectively improve the viscoelastic behavior of the materials.

The sensor response time is also a crucial parameter influencing the overall performance. Fig. 4 (d) presents the response times within three cycles when the sensor is subjected to a 10 kPa pressure. The two insets are the enlargements of the curves of the first loading and third unloading. The experiment results revealed that the sensor exhibited an ultrafast response time of 25 ms, which is less than the response time of the human skin (30–50 ms) [34]. This is because the air gaps in the fiber layer rapidly expel air when they are compressed. Moreover, when the pressure is released, the arrayed microcylinders embedded in the fiber layer rapidly expand the structure and restore the compressed fiber layer to its previous state within 25 ms. This ultrafast response time enables the sensor to accurately respond with the least delay.

In this study, a dual-layer dielectric structure comprising an electrospun fiber and a microcylinder array was used to develop a capacitive pressure sensor. When low pressure is applied to the sensor, the air inside the fiber layer is squeezed out, causing the electrode spacing to change. As the load is increased, the microcylinder structure is embedded into the fiber layer, producing bending deformation under continuous squeezing. In addition to changing the electrode spacing, this causes the fiber and microcylinder to be more closely combined. The dielectric coefficient of the dielectric layer will simultaneously increase due to a large amount of air being squeezed out, thereby increasing the capacitance change. After the loading is relieved, these bent and deformed cylinders quickly bounce due to the high PDMS strength. This makes the compressed fiber expand, and air is infused into the porous fiber layer and the fluffy state is recovered. Thus, the shortcomings of the slow recovery time of the pure fiber dielectric layer are improved.

The response-recovery time test in Fig. 4 (d) shows that the proposed sensor has a fast recovery time of 25 ms, which is the same as the response time. Reference [35] used a pure fiber as a dielectric layer of the flexible capacitive sensor and yielded a recovery time of 29 ms, which is slower than that of our study (25 ms). The recovery time of the pure fiber structure becomes slower because of internal friction. The restored fluffy fiber layer is mainly attributed to elastic recovery and air infiltration of the fiber layer. The aforementioned result denotes that the proposed sensor has high structural stability during the loading–unloading process and successfully reduces the internal friction effect of the dielectric material through the elastic force of the microcylinder. Consequently, the integration of electrospun fiber and microcylinder array produces a synergistic effect and ultimately improves the performance of the sensor.

Durability and reliability are also crucial parameters influencing the performance of a flexible pressure sensor; they were evaluated through long-period loading–unloading cycle testing. Fig. S5 shows a machine with a crank-slider mechanism that was designed and assembled to evaluate the durability and reliability of the developed sensor. The sensor was placed on an experiment platform, and an electric motor propelled the crank-slider mechanism to repeatedly strike the sensor at a fixed distance of 5 cm over a long period. Fig. 5 (a) shows the curve of the 10,000th loading–unloading pressure cycle of the sensor; its corresponding peak value pressure was about 10 kPa. In addition to compression cycle testing, the flexibility and stability of the sensor were evaluated through bending cycle testing. Fig. 5 (b) shows that even after 5000 bending–unbending cycles at 60°, the capacitance signal output of

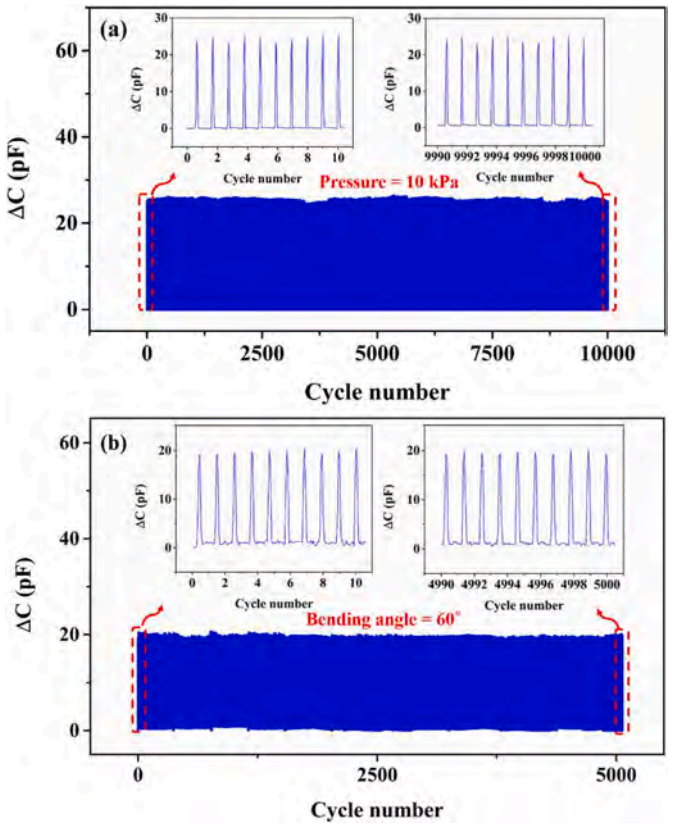

Fig. 5. Stability test under (a) pressure of 10 kPa and (b) bending angle of 60°. The partially magnified pictures show the capacitance change curves for different cycle stages.

the sensor still stayed stable. The partially magnified pictures show the changed capacitance curves for the first ten and last ten cycles. The results indicate that the sensor has an approximately stable signal output throughout the testing cycles. These durability tests demonstrate that the sensor fabricated herein has highly reproducible capacitance responses, even after 10,000 high-pressure cycles at 10 kPa and 5000 bending cycles at 60°. This implies that the developed sensor does not easily succumb to mechanical fatigue or signal attenuation, which corroborates their potential application in wearable technology.

Moreover, the proposed sensor showed a stable signal output after a long cycle test. As shown in Fig. 5 (a and b), no capacitance signal drift or attenuation was found within 10,000 compression and 5000 bending cycles. This implies that the internal material did not cause excessive mechanical damage, indirectly denoting that the fiber layer and microcylinder were not separated due to long-term compression or bending. If the internal dual-layer structure is separated, misalignment will occur and cause an increase in the internal friction and a significant signal variation will occur. Reference [28] indicated that if the internal structure is separated and misaligned, the damage caused by the internal friction will cause stress concentration, thereby reducing the actual pressure on the entire surface and causing serious signal attenuation. Herein, this phenomenon of signal variation and attenuation does not occur after long cycle tests, demonstrating that the microcylinder and electrospun fiber layer as a whole does not separate.

3.4. Evaluation of wearability and applicability

To verify whether the proposed flexible pressure sensor can be used in wearable technology to monitor physiological signals in humans, various tests such as pulse measurement, wrist bending, palm opening and closing, walking exercises, breathing tests, and acoustic vibrations were conducted. According to the test requirements, sensors with dimensions of 1.5 cm × 1.5 cm were attached to specific body parts to collect the capacitance signals due to physiological change. For example, to test weak pulse signals in the human body, the sensor was affixed to the wrist with clear tape (Fig. 6 (a)). The test subject was a healthy 22-year-old man. Based on the results, under normal circumstances, the sensor collected 12 pulse signals within 10 s, corresponding to a heart rate of 72 beats/min. The enlarged signal graph in Fig. 6 (b) clearly shows a complete heartbeat cycle formed from distinguishable systolic and diastolic waves in the heartbeat waveform. This shows that the proposed pressure sensors can immediately and accurately detect even weak pulse signals. The proposed sensors are influenced by noise (about 0.0–0.15 pF), as shown in Fig. 4 (b). However, when measuring human physiological signals, such as pulse, the lowest capacitance change is about 0.25 pF (signal-to-noise ratio > 1). The effect of noise on the cardiogram signal in Fig. 6 (a and b) is almost negligible. Thus, when the proposed sensors were used as a wearable device, they still clearly perceived bio-related signals even if some noise was present.

In addition to heart rate monitoring, sensors were attached to the elbow, palm, and heel to capture capacitance responses when bending elbows (Fig. 6 (c)), opening and closing palms (Fig. 6 (d)), and walking or running (Fig. 6 (e)); that is, signals were detected when the body was in motion. The test subject was a healthy 21-year-old woman. Initially, sensors were attached with clear tape to the side of her bent elbow and the outside of her wrist with her palm opened. The sensors were initially in an uncompressed state, and therefore, almost no change in the capacitance value was detected. However, when the elbow was extended or when the palm was clenched, the sensor was compressed by the muscles, affording relatively obvious and reproducible capacitance changes. Fig. 6 (e) displays the capacitance responses while walking at different speeds; when the test subject stood still, the capacitance response was maintained at approximately 43 pF. When the subject began to walk slowly, the capacitance response exhibited obvious frequency difference, and the average ΔC was about 49 pF. Furthermore, when the subject was running fast, because the heel exerted greater pressure on the capacitor, a higher average ΔC of about 55 pF was obtained with a faster capacitance response. These test data confirm that the proposed sensors are very sensitive toward the detection of human body movements.

Breathe monitoring is a key aspect in health monitoring. To test the sensitivity of the proposed sensors to breathing, a sensor was attached to the exhalation valve of a 3 M gas mask (Fig. 7 (a)). The test was conducted on a healthy 25-year-old man. The black curve represents the capacitance response during normal-state breathing, and the red curve represents the capacitance response during breathing after vigorous exercise. Compared to the curve of normal-state breathing, the curve for breathing after vigorous exercise showed evidently greater oscillations and frequency in the capacitance response, and the signal was highly reproducible. This verifies that the sensor can detect slight changes in the gas pressure during breathing. Furthermore, the sensor was attached to speakers to test the sensitivity to slight changes in acoustic vibrations (Fig. 7 (b)). When music was played, the sensor produced capacitance changed in response to sonic vibrations. To test the signal reproducibility, music was played twice; the obtained capacitance changes were basically the same, indicating that the sensor has not only high signal reproducibility but also outstanding sensitivity and stability. These results indicate that the sensor yields favorable responses when the body's posture greatly changes as well as when measuring pulse, breathing, and acoustic signals that require high sensitivity. Thus, the proposed sensors have massive potential for wearable sensors in future applications.

To study the capacitance changes afforded by the sensor when grabbing different objects, a robotic arm (xArm 6, Ufactory Co., Ltd, China) was used to perform real-time measurements while grabbing cuboids, cylinders, and spheres. Fig. 8 (a) presents the robotic arm. Fig. 8 (b) shows that the sensor was attached to the finger of the pneumatic gripper, and the gripper outputted the same force. According to the

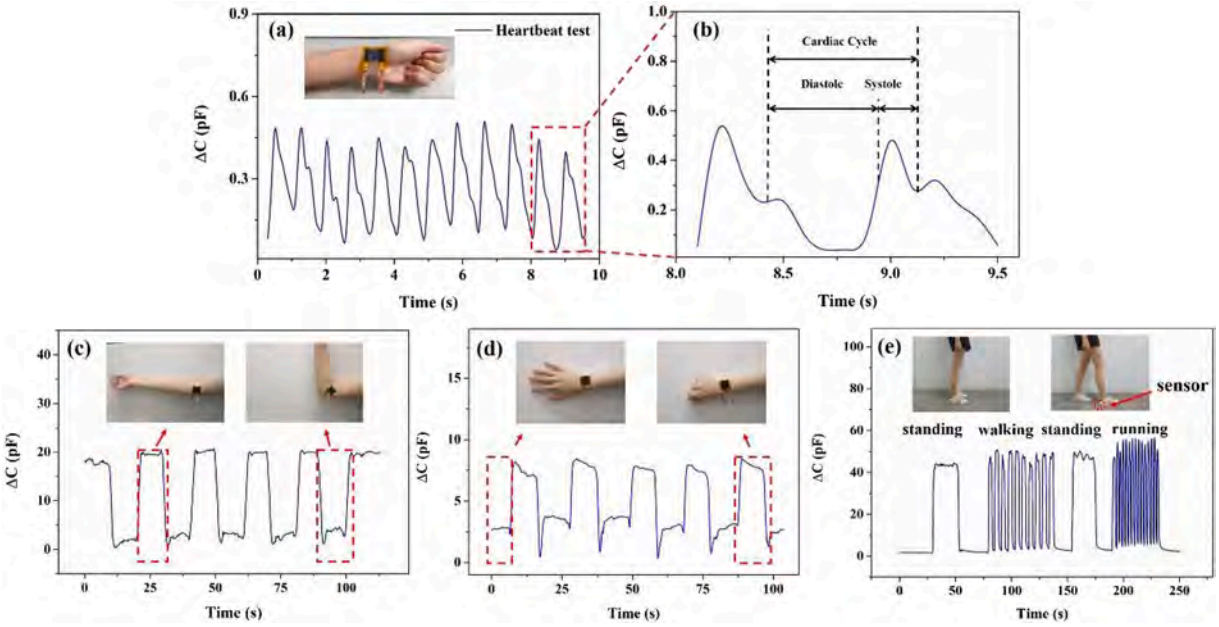

Fig. 6. The real-time monitored capacitive responses of (a) the physical force of a heartbeat under normal condition, (b) magnified view of waveform (a), (c) the arm motion, (d) the palm motion, and (e) the foot motion. Insets indicate that the sensors are attached to different positions of the human body.

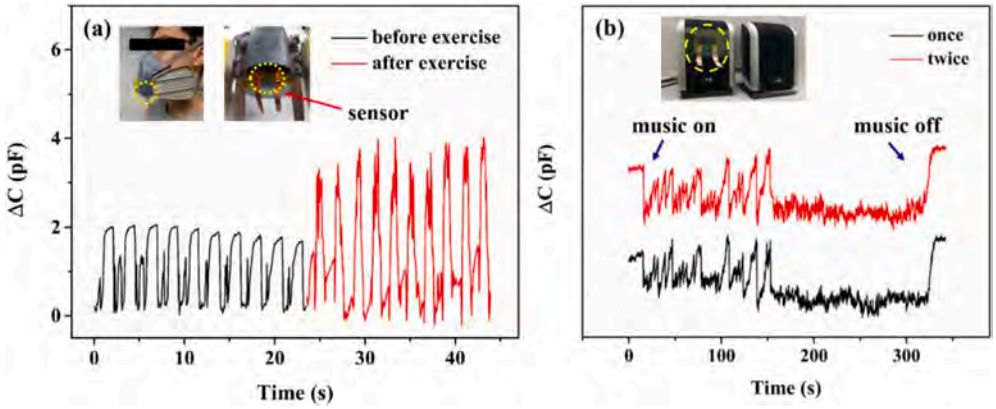

Fig. 7. The real-time monitored capacitive responses (a) when the sensor is attached to the mask before and after exercise and (b) the acoustic vibrations from a piece of music.

experiment results, although the robotic arm gripped a box, glass bottle, or ping-pong ball with the same clamping force of 50 N, the resulting capacitance responses differed (Fig. 8 (c)). When a spherical object was in point contact with the gripper, the capacitance response was a regular square wave. When the gripper was in contact with a cylindrical or rectangular object, they are in line or surface contact; therefore, distinct objects afford different capacitance output responses. Moreover, the two fingers of the gripper are not parallel when open. They contact the object and become gradually parallel during the closing process, and the changing contact area causes the capacitance response variation and forms an imperfect square wave. This verifies that the proposed sensor yields different capacitance responses when subjected to compression from different objects. Thus, it has great potential for application to nonliving objects similar to robotic arms.

3.5. Spatial compression distribution of an arrayed sensor

To simulate real-world sensing applications, the sensor must be matrixed for detecting a large-area spatial pressure. A sensor array of 6 × 6 pixels was constructed; it comprised two sheets of PI film with six copper wires as the top and bottom conductive electrodes. It was combined with a dual-layer PVDF fiber/PDMS microcylinder dielectric structure. This arrangement is similar to biological skin and can more effectively identify the overall pressure distribution. It reflects the corresponding capacitance changes based on weight compression. When two objects with different weights (a round tape weighing 4 g (Fig. 9 (a)) and a square 9 V battery weighing 35 g (Fig. 9 (c)) were placed on the sensor array, the capacitance values of the sensor varied with changes in weight in different regions, as shown in Fig. 9 (b) and (d), respectively. This arrayed sensor could accurately map the distribution of the capacitance responses corresponding to the shape of the objects. Furthermore, the compressed and uncompressed regions exhibited obviously different capacitance changes and could be easily distinguished. If a smaller sensor is used and the pixel is increased, such a sensor array could further improve the resolution of object shape recognition.

Presently, most studies on capacitive pressure sensors have only investigated single material and structure or two types of heterogeneous materials to form a single structure. The flexible capacitive pressure sensors with a dual-layer dielectric structure of PVDF fiber and PDMS

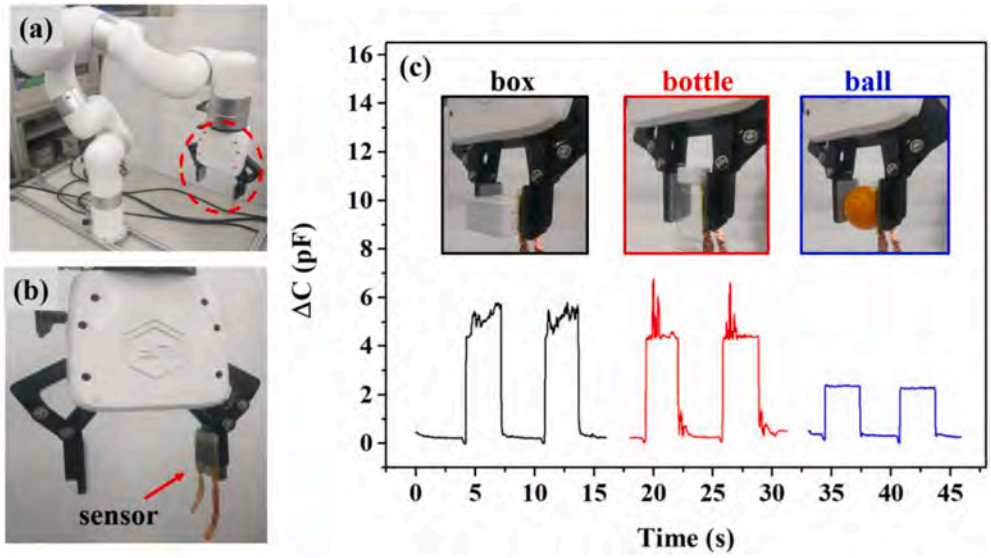

Fig. 8. Real-time monitoring of a robotic arm grabbing objects. (a) Digital photo of the robotic arm. (b) Magnified view of the claw with an attached sensor. (c) The capacitive responses when the claw grabs the box, bottle, and ball.

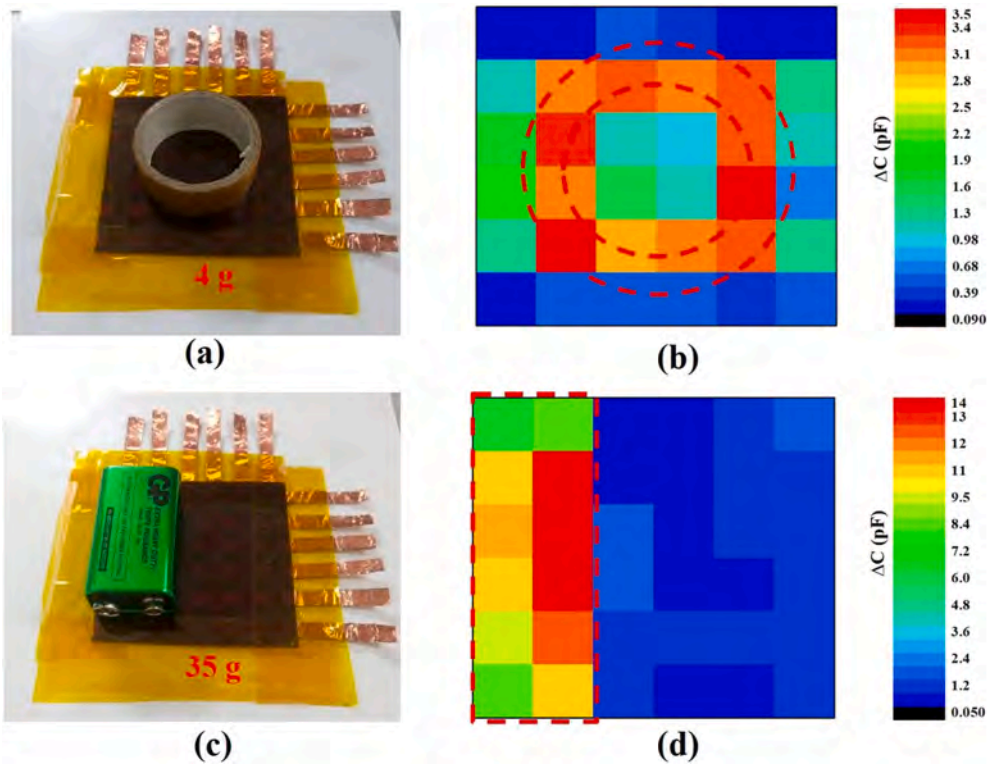

Fig. 9. (a, c) Digital photo of the pressure detection from different objects and shapes. (b, d) Readouts of the related pressure distributions based on the detection setup from (a, c).

microcylinder developed herein exhibited outstanding performance under various experimental conditions. Table 1 presents a comparison of the proposed sensor with other capacitive pressure sensors in literature [23,27–29,33,35–40]. The sensitivities of single-structure sensors range from 0.023 to 0.55 kPa^{-1} [23,28,29,36,37,40]. The proposed sensor affords a sensitivity of 0.6 kPa^{-1} with a heterogeneous dual-layer dielectric structure. Some previous studies afford higher sensitivities [27,33,35,38,39], but in terms of working pressure, the sensors proposed herein have a larger pressure range of 0–7 kPa than that of most current sensors. Moreover, they afford a high sensitivity of 0.51 kPa^{-1} at a medium pressure range of 7–15 kPa, and a sensitivity of 0.03 kPa^{-1} at a high pressure range of 15–50 kPa, as shown in Fig. S4.

Pyramid structures have been commonly utilized to fabricate pressure sensors, demonstrating several advantages, e.g., simple fabrication process and good adjustable sensitivity. However, compared to the proposed cylinder structure, they still possess some drawbacks. First, to manufacture the template of replicating PDMS structure, the template with inverted-pyramid structures must undergo some complicate procedures, such as thin film deposited as etching mask, lithography process for patterning, reactive ion etching (RIE) for forming an etch

Table 1
Comparison of the maximum sensitivity and working pressure of different types of dielectric layers.

Reference	Dielectric material	Dielectric layer structure	Maximum sensitivity (kPa^{-1})	Working pressure (kPa)
[23]	PDMS	Pyramids	0.55	0–2
[27]	PDMS/ PVDF	Micro-convex	30.20	0–0.13
[28]	PDMS	Tilted micropillar	0.42	0–1.5
[29]	P(VDF-TrFE)*1	Double-sided nanopillars	0.35	0–2
[33]	PVDF/ BTO*3	Micro-wrinkle	4.90	0–2.5
[35]	PVDF/ CNTs*5	Fiber	0.99	0–1
[36]	PDMS	Porous structure	0.023	0–200
[37]	PDMS	Porous structure/ microsphere	0.124	0–15
[38]	PDMS	Micro-wrinkle	1.62	0–0.2
[39]	PDMS/ CCP*2	Porous structure	1.10	0–10
[40]	PVDF/ CIP*4	Cilia array	0.28	0–10
This work	**PVDF/ PDMS**	**Fiber/ microcylinder**	**0.60**	**0–7**

*1 Poly(vinylidene fluoride-trifluoroethylene) (P(VDF-TrFE)).
*2 Carbon conductive paste (CCP).
*3 $BaTiO_3$ (BTO).
*4 Carbonyl iron particles (CIP).
*5 Carbon nanotubes (CNTs).

window, KOH wet chemical etching, and etching mask removal. However, the template with different aspect-ratio microhole structures can be easily obtained by adjusting the thickness of the photoresist and the aperture of the photomask using only the lithography process. Therefore, the fabrication of the microcylindrical PDMS structures is simpler and faster than that of the pyramid PDMS structure, and the size controllability is also easier.

Second, in term of performance, the pyramid structure comprises a cone-shaped feature. This dielectric layer used in the sensor will improve the sensitivity. As reference [23] in Table 1, the dielectric layer of the pyramid structure has a high sensitivity of 0.55 kPa^{-1}, but its effective pressure range is only 0–2 kPa due to its low aspect ratio. Compared to the performance of only the microcylinder structure (0.39 kPa^{-1} and 0–6 kPa), the pyramid structure shows higher sensitivity but lower pressure range and longer recovery time (>500 ms) [23]. This study proposes a complementary structure wherein fiber and microcylinder are integrated as a dielectric layer. The higher aspect-ratio microcylinder can be effectively embedded in the fiber layer under applied pressure. After the pressure is released, the elastic force of the microcylinder allows the sensor to quickly return to its initial state, improving the recovery time afforded using only the fiber layer. If the pyramid structure is integrated with the fiber layer, it can be effectively embedded into the fiber when the sensor is compressed. However, their return to the initial state is predicted to be slow, which will result in a long recovery time. Compared to the performance of the cylinder structure integrated with the fiber layer (0.6 kPa^{-1}, 0–7 kPa, and 25 ms), the pyramid structure exhibits slightly less sensitivity, pressure range, and recovery time, which causes application limitation in future wearable sensing fields.

In our study, the unique fiber and cylinder integrated dual-layer structure improves the sensitivity to pressure as well as enables the operation of the sensor in a broader pressure range. Moreover, it has a rapid response time of 25 ms, ultralow LOD of 0.065 Pa, and high durability and high reliability without any signal attenuation up to 10,000 load/unload cycles and up to 5000 bending/unbending cycles. Thus, the developed sensors with a dual-layer dielectric structure perform better than most single-structure sensors; such sensors are predicted to have excellent application potential in wearable devices and human–machine interfaces as well as in large-area shapes. These advantages allow the proposed sensor to have versatile potential applications in the future.

4. Conclusions

A composite dielectric layer with a PVDF electrospun fiber and PDMS microcylinder structure was developed herein and applied to fabricate a new type of flexible capacitive pressure sensor. The structured dielectric layer for this sensor can be prepared using a simple and cost-effective method. Experiment results verify that the sensor has multisectional tunable sensitivity of 0.6 kPa^{-1} (0–7 kPa), 0.51 kPa^{-1} (7–15 kPa), and 0.03 kPa^{-1} (15–50 kPa); a rapid response time of approximately 25 ms; an ultralow LOD of 0.065 Pa; and a high durability and high reliability with no signal attenuation up to 10,000 load/unload cycles and up to 5000 bending/unbending cycles. Furthermore, this device was successfully used to measure physiological and movement signals, such as pulse, limb movement, breathing, and acoustic vibrations, in humans; thus, the sensor has potential for use in wearable applications. Grip perception experiments were performed by attaching the sensor to a mechanical gripper; the results reveal that the device exhibited different capacitance responses when the robotic arm gripped objects of different shapes, proving that the sensor has the ability to identify basic shapes of objects. Finally, the sensor was arranged in a 6 × 6 array, and the pressure distribution was successfully mapped on a plane. Based on the above findings, the proposed flexible capacitive pressure sensor has massive potential in future applications for use in wearable fitness trackers, robotic arms, human–machine interfaces, and flexible touch screens.

Declaration of competing interest

The authors declare that they have no known competing financial interests or personal relationships that could have appeared to influence the work reported in this paper.

Acknowledgments

We thank the Ministry of Science and Technology of Taiwan for financially supporting this research under the projects MOST 108-2221-E-003-013 and MOST 108-2622-E-003-002-CC3. Moreover, Professor Hsin-Han Chiang of Department of Electrical Engineering at National Taiwan Normal University, is commended for his assistance in evaluating the sensor performance using the robotic arm.

Appendix A. Supplementary data

Supplementary data to this article can be found online at https://doi.org/10.1016/j.orgel.2021.106290.

References

[1] S. Takamatsu, et al., Wearable keyboard using conducting polymer electrodes on textiles, Adv. Mater. 28 (22) (2016) 4485–4488.
[2] Y. Pang, et al., Epidermis microstructure inspired graphene pressure sensor with random distributed spinosum for high sensitivity and large linearity, ACS Nano 12 (3) (2018) 2346–2354.
[3] Y. Wu, et al., Insect-scale fast moving and ultrarobust soft robot, Sci Robot 4 (32) (2019), eaax1594.
[4] C. Pang, et al., Highly skin-conformal microhairy sensor for pulse signal amplification. Adv. Mater. 27 (4) 2015 2634−640.
[5] S. Choi, et al., Recent advances in flexible and stretchable bio-electronic devices integrated with nanomaterials, Adv. Mater. 28 (22) (2016) 4203–4218.
[6] S.W. Park, et al., Development of wearable and flexible insole type capacitive pressure sensor for continuous gait signal analysis, Org. Electron. 53 (2018) 213–220.
[7] S. Gong, et al., A wearable and highly sensitive pressure sensor with ultrathin gold nanowires, Nat. Commun. 5 (1) (2014) 1–8.

[8] C. Pang, et al., A flexible and highly sensitive strain-gauge sensor using reversible interlocking of nanofibres, Nat. Mater. 11 (9) (2012) 795–801.
[9] H. Kim, et al., Chemically designed metallic/insulating hybrid nanostructures with silver nanocrystals for highly sensitive wearable pressure sensors, ACS Appl. Mater. Interfaces 10 (1) (2018) 1389–1398.
[10] C. Dagdeviren, et al., Recent progress in flexible and stretchable piezoelectric devices for mechanical energy harvesting, sensing and actuation, Extreme Mech. Lett. 9 (2016) 269–281.
[11] J. Park, et al., Fingertip skin–inspired microstructured ferroelectric skins discriminate static/dynamic pressure and temperature stimuli, Sci. Adv. 1 (9) (2015), e1500661.
[12] S. Xu, et al., Flexible piezoelectric PMN–PT nanowire-based nanocomposite and device, Nano Lett. 13 (6) (2013) 2393–2398.
[13] J. He, et al., Recent advances of wearable and flexible piezoresistivity pressure sensor devices and its future prospects, J. Materiomics. 6 (1) (2020) 86–101.
[14] H.J. Kim, et al., Bacterial nano-cellulose triboelectric nanogenerator, Nano Energy 33 (2017) 130–137.
[15] Y. Chi, et al., Rice paper-based biodegradable triboelectric nanogenerator, Microelectronic Eng 216 (2019) 111059.
[16] W. Paosangthong, et al., Recent progress on textile-based triboelectric nanogenerators, Nano Energy 55 (2019) 401–423.
[17] S. Lee, et al., Development of battery-free neural interface and modulated control of tibialis anterior muscle via common peroneal nerve based on triboelectric nanogenerators (TENGs), Nano Energy 33 (2017) 1–11.
[18] Z. He, et al., Capacitive pressure sensor with high sensitivity and fast response to dynamic interaction based on graphene and porous nylon networks, ACS Appl. Mater. Interfaces 10 (15) (2018) 12816–12823.
[19] S.H. Cho, et al., Micropatterned pyramidal ionic gels for sensing broad-range pressures with high sensitivity, ACS Appl. Mater. Interfaces 9 (11) (2017) 10128–10135.
[20] Y. Zang, et al., Advances of flexible pressure sensors toward artificial intelligence and health care applications, Mater. Hori. 2 (2) (2015) 140–156.
[21] K. Lee, et al., Rough-surface-enabled capacitive pressure sensors with 3D touch Capability, Small 13 (43) (2017) 1700368.
[22] X. Chen, et al., High-performance piezoelectric nanogenerators with imprinted P (VDF-TrFE)/$BaTiO_3$ nanocomposite micropillars for self-powered flexible sensors, Small 13 (23) (2017) 1604245.
[23] S.C. Mannsfeld, et al., Highly sensitive flexible pressure sensors with microstructured rubber dielectric layers, Nat. Mater. 9 (10) (2010) 859–864.
[24] B.C.K. Tee, et al., Tunable flexible pressure sensors using microstructured elastomer geometries for intuitive electronics, Adv. Funct. Mater. 24 (34) (2014) 5427–5434.
[25] C.M. Boutry, et al., A sensitive and biodegradable pressure sensor array for cardiovascular monitoring, Adv. Mater. 27 (43) (2015) 6954–6961.
[26] X. Zeng, et al., Tunable, ultrasensitive, and flexible pressure sensors based on wrinkled microstructures for electronic skins, ACS Appl. Mater. Interfaces 11 (23) (2019) 21218–21226.
[27] Y. Xiong, et al., A flexible, ultra-highly sensitive and stable capacitive pressure sensor with convex microarrays for motion and health monitoring, Nano Energy 70 (2020) 104436.
[28] Y. Luo, et al., Flexible capacitive pressure sensor enhanced by tilted micropillar arrays, ACS Appl. Mater. Interfaces 11 (19) (2019) 17796–17803.
[29] Y. Guo, et al., Anodized aluminum oxide-assisted low-cost flexible capacitive pressure sensors based on double-sided nanopillars by a facile fabrication method, ACS Appl. Mater. Interfaces 11 (51) (2019) 48594–48603.
[30] J. Yang, et al., Flexible, tunable, and ultrasensitive capacitive pressure sensor with microconformal graphene electrodes, ACS Appl. Mater. Interfaces 11 (16) (2019) 14997–15006.
[31] S. Baek, et al., Flexible piezocapacitive sensors based on wrinkled microstructures: toward low-cost fabrication of pressure sensors over large areas, RSC Adv. 7 (63) (2017) 39420–39426.
[32] S.G. Yoon, et al., Highly sensitive piezocapacitive sensor for detecting static and dynamic pressure using ion-gel thin films and conductive elastomeric composites, ACS Appl. Mater. Interfaces 9 (41) (2017) 36206–36219.
[33] L. Ma, et al., Highly sensitive flexible capacitive pressure sensor with a broad linear response range and finite element analysis of micro-array electrode, J. Materiomics. 6 (2) (2020) 321–329.
[34] Z. Bao, et al., Skin-inspired organic electronic materials and devices, MRS Bull. 41 (11) (2016) 897.
[35] X. Yang, et al., A flexible capacitive sensor based on the electrospun PVDF nanofiber membrane with carbon nanotubes, Sens. Actuator. A Phys. 299 (2019) 111579.
[36] S. Li, et al., Capacitive pressure sensor inlaid a porous dielectric layer of superelastic polydimethylsiloxane in conductive fabrics for detection of human motions, Sens. Actuator. A Phys. 312 (2020) 112106.
[37] Y. Jung, et al., A highly sensitive and flexible capacitive pressure sensor based on a porous three-dimensional PDMS/microsphere composite, Polymers 12 (6) (2020) 1412.
[38] B. Zhuo, et al., High sensitivity flexible capacitive pressure sensor using polydimethylsiloxane elastomer dielectric layer micro-structured by 3-D printed mold, IEEE J. Electron. Devices. Soc. 5 (3) (2017) 219–223.
[39] P. Wei, et al., Flexible capacitive pressure sensor with sensitivity and linear measuring range enhanced based on porous composite of carbon conductive paste and polydimethylsiloxane, Nat. Nanotechnol. 30 (45) (2019) 455501.
[40] Q. Zhou, et al., A bio-inspired cilia array as the dielectric layer for flexible capacitive pressure sensors with high sensitivity and a broad detection range, J. Mater. Chem. A. 7 (48) (2019) 27334–27346.